What data are most valuable to screen ionic liquid entrainers for hydrofluorocarbon refrigerant reuse and recycling?

Alejandro Garciadiego, Bridgette J. Befort, Gabriela Franco, Mozammel Mazumder, and Alexander W. Dowling*

Department of Chemical and Biomolecular Engineering University of Notre Dame, Notre Dame, IN 46556

E-mail: adowling@nd.edu

Abstract

Separating azeotropic mixtures of hydrofluorocarbons (HFCs) for reuse and recycle is environmentally and economically imperative. While ionic liquid (IL)-enabled HFC separations show promise, Edisonian trial-and-error screening for the optimal IL entrainer is intractable and expensive. Here we propose an open-source, equation-oriented modeling framework to rapidly translate HFC/IL solubility data into regressed thermodynamic models which can be used for process design under uncertainty and rapid IL screening. Moreover, we use data science and process systems engineering tools to contemplate which data are the most valuable for IL screening. We find that binary solubility data collected at multiple temperatures is adequate for separation process design and newly available ternary solubility measurements should be reserved for validation. Additionally, we use uncertainty quantification analyses to show up to 10% experimental error is acceptable for IL screening decisions. Informed by these results, we recommend a multi-step workflow for IL screening.

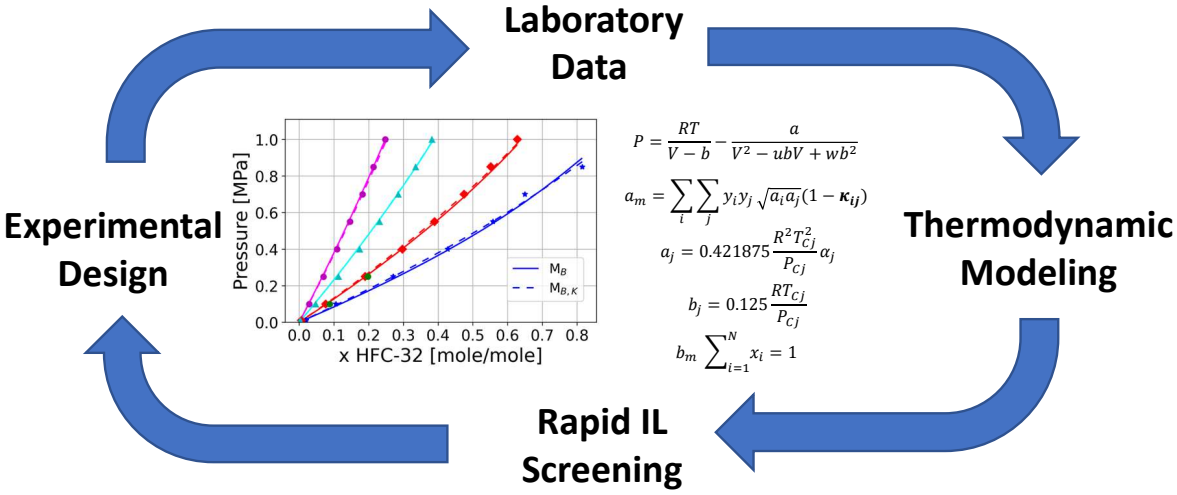

Graphical abstract

Introduction

Due to their high ozone depletion potential, chlorofluorocarbon (CFC) refrigerants were phased out under the 1987 Montreal Protocol and replaced by their close molecular relative, hydrofluorocarbons (HFCs), which had similar excellent refrigeration properties. However, more recently, many of these second generation HFC refrigerants have been shown to have high global warming potentials (GWPs), caused by their ability to block infrared radiation[1] and extended atmospheric lifetimes, ranging from five to forty-seven years.[2,3] In fact, 2019 United States (US) industrial HFC emissions accounted for more than 175 million metric tons of carbon dioxide equivalents in the atmosphere.[4] This alarming environmental impact has sparked renewed global concern resulting in fresh mandates for environmentally detrimental refrigerant phase out. For example, the 2016 Kigali Amendment[5] to the Montreal Protocol aims to cooperatively achieve an 85% reduction of HFC use by 2036 among industrialized countries. The American Innovation and Manufacturing (AIM) Act of 2020[6] authorized

the U.S. Environmental Protection Agency (EPA) to limit HFC production to 15% of the present values by 2036.[6] In addition to environmental incentives, the EPA estimates this future reduction of fluorinated gas emissions can have an annual social benefit of up to $2.8 billion.[7] Also important to consider is the huge economic value of HFCs. For example, there are approximately 100 million kilograms of HFC-32, a low GWP HFC used in many refrigerant mixtures, in global circulation worth around half a billion dollars.[8]

The combined environmental, social, and economic impact of HFC refrigerants makes it imperative to develop a sustainable path forward for their phaseout. Fortunately, there remain new opportunities to reuse low GWP HFCs, either as pure refrigerants[9] or in next generation refrigerant mixtures,[10] and recycle high GWP HFCs into new products. However, complicating this phaseout and transition to more environmentally-friendly chemicals is the fact that most refrigerants are manufactured and deployed as azeotropic mixtures of HFCs. While this azeotropic nature creates an ideal refrigerant with a single boiling point that will not separate in a leak, conventional technologies, i.e., distillation, become impractical when separating the components of these mixtures at the end of their utility.

Ionic liquid (IL) entrainers can effectively separate HFC mixtures, overcoming the energy costs of traditional separation technologies.[11–13] Over the past eighteen years, IL and HFC systems have been studied in a variety of contexts including the characterization of their individual and mixture physical properties[14–24] and their use in extractive distillation, membrane, and adsorption separation processes.[12] More recent work has used data generated from these studies to regress thermodynamic models then perform process design, optimization, technoeconomic analyses, and life cycle assessments for IL-enabled HFC separation schemes.[13,25–27] However, because millions of theoretical ILs are available, each with unique properties, trial-and-error molecular and process design is intractable since each HFC within a refrigerant blend exhibits a different boiling point and solubility with an IL.[28] This necessitates a framework which integrates experiments, mathematical models, and computational optimization to concurrently design ILs and separation processes for azeotropic HFC refrig-

erant mixtures. Thus, several opportunities remain to explore the intersection between IL discovery and design, thermophysical property measurements, and process engineering.

Here, we integrate published HFC/IL solubility data and process systems engineering approaches to answer the question: *what data are most valuable to screen IL entrainers for HFC reuse and recycling?* We investigate the use of first-of-their-kind thermophysical property measurements of ternary mixtures of HFCs and ILs, i.e., two HFCs mixed with an IL,[29] within an HFC separation process design framework, determining how to best incorporate these new measurements to effectively screen ILs for use as entrainers. This enables us to begin to bridge the gap between experimental thermophysical property characterization, which is often driven by scientific goals, and process design decisions, which are guided by engineering principles, by addressing the following questions:

- What is the best way to use the new HFC/IL ternary mixture data to accelerate the design of HFC separation systems and the screening of IL entrainers?
- What is the uncertainty in property predictions for regressed thermodynamic models using various types of HFC/IL mixture data (e.g., binary versus ternary mixture data at single versus multiple temperatures)? How does this uncertainty propagate through process design calculations?
- What experimental precision for HFC/IL mixture data is sufficient to screen IL entrainers?

We propose an open-source, equation-oriented modeling framework to rapidly translate HFC/IL mixture data into regressed thermodynamic models for rapid IL screening. In contrast to prior work, this framework propagates uncertainty in experimental data to process-level physical properties. This allows us to evaluate precision between experimental measurements versus model predictions, providing the opportunity to systematically guide laboratory and simulation experiments on the data types and accuracy that are needed for HFC separation process design and IL screening.

Literature review

Azeotropic distillation process design and entrainer screening

Separating mixtures with very close boiling points, such as azeotropic HFC mixtures, using conventional distillation requires a large number of trays, making the separation energy intensive and uneconomical.[30] To overcome this challenge, azeotropic and extractive distillation schemes have been used to separate these types of mixtures for more than 90 years.[12] Introducing an entrainer, i.e., a mass separating agent, to a close-boiling mixture creates a new mixture comprised of the entrainer and one of the original azeotropic mixture components. This new mixture, which may form its own azeotrope, has a different boiling point, breaking the original azeotrope to allow separation.[31] Techniques to identify ideal entrainers include using the molecular structure,[32] residue curve maps,[33] volatilities,[34] process simulations,[35] and entrainer selection rules developed by Rodrıguez-Donis *et al.*[36] Yet, the search for entrainers is challenging and time consuming. For example, optimization of entrainers for separating water and ethanol has been ongoing since the 1930s.[37–39] However, for HFC systems especially, environmental regulations and global economics necessitate rapid innovation within the next decade.

Ionic liquids as entrainers

ILs are generally defined as organic salts with melting points below 100°C that are soluble with a wide range of organic compounds.[40,41] ILs exhibit many traits which make them ideal entrainers. For example, ILs have tunable structure-property relationships such that the cation and anion which comprise the molecule can be selected from among a variety of options to achieve a specific chemical purpose. ILs have negligible vapor pressure which leads to easy recovery and essentially no contamination of products within a separation scheme, allowing ILs to be recycled in a separation process, reducing material demands and improving the separation economics.[42] ILs also have been shown to have excellent ability to separate

a wide range of azeotropic and close-boiling mixtures.[13,43–45] Other convenient properties of ILs include their existence in a liquid state over a wide temperature range and their high thermal and chemical stability.[46–49] Since the feasibility of using ILs in extractive distillation schemes[11,12] was shown in the early 2000s, many studies have evaluated their properties in mixtures with fluorinated refrigerants[14–24] and examined their use in HFC separations.[13,25] More recently, Asensio-Delgado *et al.*[50] created an extensive database with more than 5000 data points of fluorinated gases and IL mixtures. Additionally, several efforts to validate ternary models of HFC/HFC/IL mixtures using binary HFC/IL data have been made.[51,52] ILs have also been the subject of computer-aided molecular design research, which has aimed to take advantage of their tunability to simultaneously design IL entrainers and optimize the separation processes in which they are used.[53,54]

Regression of thermodynamic models

Because equations of state (EoS) are continuous and differentiable functions, they are well-suited for computer-aided process design and optimization.[55–57] EoS models, including van der Waals,[58,59] Peng-Robinson,[60] Redlich-Kong,[19,20] and soft-SAFT EoS,[61] have been shown to reliably predict thermodynamic properties of HFC and IL mixtures. Yet, many of these models include parameters which must be calibrated from data before they are used in process design. These parameters are often fitted using a minimizing least-squares approach[62,63] involving the pressure of the system.[19,20,58–60] However, different objective functions, such as those involving liquid or vapor compositions, can be utilized in practice and may provide different parameter values.[64]

There is a rich history of nonlinear parameter estimation within the chemical engineering discipline and, more specifically, thermodynamics community. It is well known that EoS parameter estimation is a nonconvex optimization problem and local optima are common and either multi-start initialization or rigorous global optimization methods are recommended.[63,65–67] Besides local minima, spurious solutions are another key challenge for EoS

calibration. Common mitigation strategies include bilevel optimization methods,[68,69] branch and bound methods,[67] or the addition of penalty terms to the optimization problem.[70] Post regression tests can be implemented, including the Gibbs tangent plane method,[71] which enforces a stable solution of the phase equilibrium problem if and only if the tangent plane lies below the Gibbs free energy surface for all compositions.

Once parameterized, EoS models are used for process design and optimization, yet thermodynamic model parameterization is often one of the most significant sources of uncertainty and risk in process design. For example, Hajipour and Satryo[72,73] show how underestimating critical temperature by 2% while fitting binary interaction parameters may produce errors of 20% to 60% in vapor pressure predictions for petroleum engineering systems. However, out of the numerous thermodynamic modeling studies for HFC/IL systems, we are aware of only two papers, co-authored by us, which investigate EoS parameter uncertainties. In Morais *et al*,[59] we use Monte Carlo techniques to calculate the uncertainty of parameters for the van der Waals EoS and describe the apparent over-parameterization of the model due to observed parameter sloppiness. In Baca *et al*,[29] we report and interpret the covariance matrix of estimated Peng-Robinson EoS parameters. However, there remains a need to understand how these uncertainties impact separation process design and IL screening decisions, which is a key contribution of this work.

Methods

To address the aforementioned gap, this paper presents an equation-oriented modeling framework to systematically translate binary or ternary vapor-liquid equilibrium (VLE) data into regressed thermodynamic and process models for rapid IL screening. Figure 1 depicts the workflow, which starts by specifying the system VLE data (Step 1) and EoS model (Step 2), which are inputs for parameter estimation (Step 3). The parameterized models are then used to make phase predictions (Step 4) and generate process designs, specifically flash calcula-

tions in this work (Step 5). Additionally, we use these parameters to calculate the pressure of the mixture to compare the quality of fit of our models (Step 6). Finally, ILs are screened for their HFC separations ability via a comparison of HFC relative volatility in the IL entrainer (Step 7) and uncertainty analysis is performed to inform experimental design (Step 8). The framework leverages tools from the open-source Institute for the Design of Advanced Energy Systems (IDAES) Integrated Platform[74] and the Pyomo Python library.[75,76] Utilizing these open-source packages for modeling and optimization facilitates validation, reproducibility, and accountability, and allows for easy extension of the framework to other systems.

As a case study, we apply this workflow to screen six ILs for the separation of HFC-32 and HFC-125, which comprise the refrigerant R-410a. The remainder of this section describes the individual steps of the workflow.

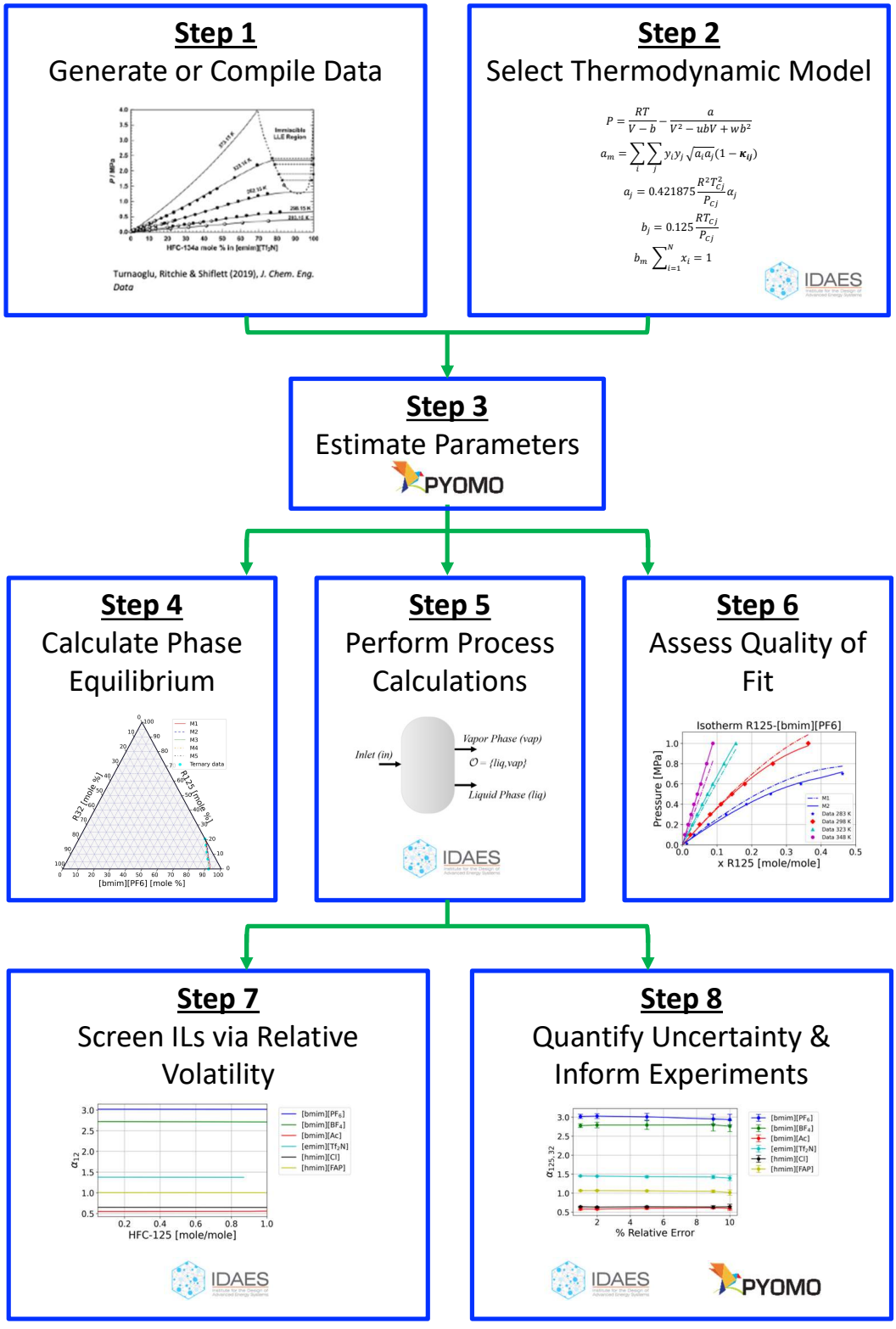

Figure 1: Open-source, equation-oriented modeling framework for HFC separation process design and IL entrainer screening.

Step 1. Generate or compile data

Based on previous studies from Morais *et al.*[59] and Baca *et al.*,[29,60] three types of data are considered in this work:

1. Binary HFC/IL solubility data for HFC-32 or HFC-125 in [bmim][PF_6], [bmim][BF_4], [emim][TF_2N], [bmim][Ac], [hmim][Cl], and [hmim][FAP] collected with a gravimetric microbalance.[18,20,59,60]

2. HFC-32/HFC-125 binary equilibrium data collected with gas chromatograph equipped with a flame ionization detector.[77]

3. Ternary mixture data for HFC-32 and HFC-125 in [bmim][PF_6] and [bmim][BF_4] collected from XEMIS and IGA gravimetric microbalances with the integral mass balance method.[29]

Step 2. Select thermodynamic model

We utilize a cubic equation of state (EoS) for this analysis as they are often used to model refrigeration systems,[19,20,58–60] and have been shown to be capable of predicting liquid/liquid regions of the phase diagram after being calibrated using only vapor/liquid region data.[78] Eventually, a soft-SAFT EoS may be implemented, which may allow the framework to have predictive capabilities.[79]

Peng-Robinson EoS

We correlate experimental data utilizing the Peng-Robinson EoS:

$$P = \frac{RT}{V-b} - \frac{a_m}{V^2 - 2b_m V - b_m^2} \tag{1}$$

where pressure P is a function of temperature T, volume V, and the intermediate variables a_m and b_m. The substance-specific parameters a_j and b_j for each component j are calculated

with:

$$a_j = 0.421875 \frac{R^2 T_{c,j}^2}{P_{c,j}} \alpha_j \tag{2}$$

$$\alpha_j = \left(1 + (1 - T_r^2)(0.37464 - 1.54226\omega_j - 0.26992\omega_j^2)\right)^2 \tag{3}$$

$$b_j = 0.125 \frac{R T_{c,j}}{P_{c,j}} \tag{4}$$

where R is the ideal gas constant, P_c and T_c are the pressure and temperature, respectively, at the critical point, and ω_j is the acentric factor. a_m and b_m are calculated with the mixing rule recommended for cubic EoS:[80]

$$a_m = \sum_i \sum_j y_i y_j \sqrt{a_i a_j} \left(1 - \kappa_{i,j}(T)\right) \tag{5}$$

$$b_m \sum_{i=1}^{N} x_i = 1 \tag{6}$$

where $\kappa_{i,j}$ is the binary interaction parameter function:

$$\kappa_{i,j}(T) = \kappa_{Ai,j} + \kappa_{Bi,j} \cdot T \tag{7}$$

Specifying $\kappa_{Bi,j} = 0$ removes the temperature dependence for Eq. (7).

Regressed models

To study the differences between the use of different combinations of binary and ternary data sets, as well as to study the influence of temperature on fitted parameters in Eq. (7), we postulate five combinations of fitting data sets and models for comparison:

- M_B: EoS parameterized with binary data without binary interaction temperature dependence, i.e., $\kappa_{Bi,j} = 0$.

- $\mathrm{M}_{B,K}$: EoS parameterized with binary data taking into account binary interaction

temperature dependence.

- M_T: EoS parameterized with ternary data without binary interaction temperature dependence, i.e., $\kappa_{Bi,j} = 0$.
- M_{BT}: EoS parameterized with binary data and ternary data without binary interaction temperature dependence. Data are weighted based on the number of observations in each data set and normalized by the average pressure.
- $M_{BT,K}$: EoS parameterized with binary data and ternary taking into account binary interaction temperature dependence. Data are weighted the same as for M_{BT}.

Here, the subscript B denotes a model was parameterized with binary data, the subscript T denotes the model was parameterized with ternary data, and the subscript BT indicates a model was parameterized with both binary and ternary data. The subscript K (for Kelvin) denotes a temperature dependence of the binary parameters, i.e., $\kappa_{Bi,j}$ was calibrated. Table 1 compactly summarizes the models.

Table 1: Postulated models to predict HFC/IL phase equilibrium.

Model	$\kappa_{Bi,j}$	**Binary data**	**Ternary data**
M_B	0	Yes	No
$M_{B,K}$	Optimized	Yes	No
M_T	0	No	Yes
M_{BT}	0	Yes	Yes
$M_{BT,K}$	Optimized	Yes	Yes

Step 3. Estimate parameters

Nonlinear least-squares optimization was performed in `Pyomo` using `parmest`[81] to calculate the binary parameters κ via Eq. (5):

$$\min_{\kappa^l \le \kappa \le \kappa^u} \quad \sum_{d=1}^{D} \left[\frac{w_d}{n_d} \sum_{i=1}^{n_d} (\hat{P}(\kappa, T_{i,d}, x_{i,d}) - P_{i,d})^2 \right] \qquad \text{s.t.} \quad \text{Eqs.} \quad (1) - (10) \tag{8}$$

Here P_i is the experimentally measured pressure value, $\hat{P}$ is the model prediction of pressure, D is the total number of data sets, n_d is the number of observations in data set d, and the weight w_d is the average pressure of the data set. Minimizing the least-squares error of the calculated pressure $\hat{P}$ and experimental pressure P is consistent with prior literature on EoS calibration for IL and HFC mixtures.[19,20,58,59] The model is constrained by Eqs. (1) to (10). With $D = 1$ and $n = 32$,where n is the number of fitted points $n = \sum_{d=1}^{D} n_d$, the model contains 434 variables and 432 equality constraints for the case in which only $\kappa_{Ai,j}$ is fit. We can estimate parameters for the full [bmim][PF_6] data set using IPOPT[82] solver and HSL (MA27)[83] in approximately 30 seconds with thoughtfully chosen initial parameter values. The bounds κ^l and κ^u were set to -3 and 3, respectively. In all obtained optimal solutions these bounds were not active.

Alternatively, we can estimate the parameters by minimizing the least squares error of the composition:

$$\begin{aligned} \min_{\kappa^l \leq \kappa \leq \kappa^u} \quad & \sum_{d=1}^{D} \left[\frac{w_d}{n_d} \sum_{i=1}^{n_d} (\hat{x}(\kappa, T_{i,d}, P_{i,d}) - x_{i,d})^2 \right] \\ \text{s.t.} \quad & \text{Eqs.} \quad (1) - (10) \end{aligned} \tag{9}$$

Here $x_{i,d}$ is the experimentally measured liquid phase composition and, $\hat{x}(\kappa, T_{i,d}, P_{i,d})$ is the model prediction of the liquid composition. With $D = 1$ and $n = 32$ the model contains 434 variables and 432 equality constraints for the two-parameter $\kappa_{Ai,j}$ system. We can estimate parameters for the full [bmim][PF_6] data set using IPOPT[82] solver and HSL (MA27)[83] in approximately 31 seconds. Although both formulations are computationally tractable, Eq. (8) is predominatenly used in previous IL literature.[19,20,29,58,59] To be consistent, Eq. (8) is used throughout the remainder of the analysis.

Step 4. Calculate phase equilibrium

We use the *phi-phi* method[84] to calculate VLE at temperature T_{eq}:

$$\Phi_{vap,i}(T_{eq}) = \Phi_{liq,i}(T_{eq}) \tag{10}$$

Here the Peng-Robinson EoS is used to calculate the fugacities of both phases, $\Phi_{vap,i}$ and $\Phi_{liq,i}$.[85] However, Eq. (10) is only valid in the two-phase region. It is relaxed as follows as part of the smooth flash formulation:[85]

$$T_1 = \max(T_{bubble}, T) \tag{11}$$

$$T_{eq} = \min(T_1, T_{dew}) \tag{12}$$

where T_1 is an intermediate variable, and T is the outlet temperature. Thus if $T < T_{bubble}$, then the VLE is calculated at T_{bubble}. Likewise if $T > T_{dew}$, then the VLE is calculated at T_{dew}. The calculation is reformulated with smooth min and max operators to improve numerical performance with derivative-based equation solving and optimization algorithms.

$$T_1 = 0.5\left[T + T_{bubble} + \sqrt{(T - T_{bubble})^2 + \epsilon_1^2}\right] \tag{13}$$

$$T_{eq} = 0.5\left[T + T_{dew} + \sqrt{(T - T_{dew})^2 + \epsilon_2^2}\right] \tag{14}$$

where $\epsilon_1 = 0.01$ and $\epsilon_2 = 5.0 \times 10^{-5}$ are smoothing parameters.[85]

Step 5. Perform Process Calculations

Shiflett and Yokozeki[13] presented an extractive distillation flowsheet that uses an IL entrainer to separate R-410A, which is a 50/50 mass% mixture of HFC-32 and HFC-125. In this extractive distillation column, HFC-125 is the top product and HFC-32 and the IL are the bottom products. The HFC-32 and IL mixture is then sent to the recycling section of the

flowsheet with two sequential flash vessels to separate HFC-32 from the IL entrainer. The IL is then recycled to the extractive distillation column. The first vessel is operated at 0.1 MPa and 371 K. With a feed composition x_{in} of 21.6 mol% of HFC-32, 0.3 mol% of HFC-125, and 78.1 mol% of [bmim][PF_6].[13] We simulate this flash vessel to illustrate the impact of data and model uncertainty on process modeling calculations. The flash is modeled as follows:

$$F_{in} = \sum_{l \in \mathcal{O}} F_l \tag{15}$$

$$F_{in} x_{in,c} = \sum_{l \in \mathcal{O}} F_l x_{l,c}, \quad \forall c \in \mathcal{C} \tag{16}$$

$$\sum_{c \in \mathcal{C}} (x_{vap,c} - x_{liq,c}) = 0 \tag{17}$$

Eq. (15) is a total mole balance that equates the inlet total molar flowrate, F_{in}, with the sum of the outlet, F_l. Eq. (16) is the component balance and equates the product of the inlet flow F_{in} and the inlet composition $x_{in,c}$ of a component c to the sum of the flow of the outlet streams F_l and the mole fraction $x_{l,c}$ of component c in the outlet streams l. Finally, Eq. (17), commonly known as the Rachford–Rice equation, ensures the sum of the differences between vapor and liquid fractions of the components, $x_{vap,c}$ and $x_{liq,c}$, must be equal to zero.

Step 6. Assess quality of fit

We utilize the mean absolute percent error (MAPE) metric to quantify the fit and the accuracy of our model predictions:

$$MAPE = \sum_{d=1}^{D} \left[\frac{1}{n_d} \sum_{i=1}^{n_d} \left| \frac{\hat{P}(\kappa, T_{i,d}, x_{i,d}) - P_{i,d}}{\hat{P}(\kappa, T_{i,d}, x_{i,d})} \right| \right] \tag{18}$$

Here we compare the accuracy of the calculated pressure $\hat{P}$ and experimental pressure P, normalizing by the number of observations n_d in data set d for all the data sets D. We calculate two types of MAPE: in-sample, which corresponds to data used for parame-

ter calibration, and out-of-sample, which corresponds to data not used for the parameter calibration.

Step 7. Screen ILs via relative volatility

Relative volatility is a good indicator of an IL's potential as an entrainer and is a popular screening metric.[34] We screen prospective ILs by calculating the relative volatility, $\alpha_{i,j}(T, P, x_{in})$, for species i relative to species j at different compositions of the species:

$$\alpha_{i,j} = \frac{y_i/x_i}{y_j/x_j} \tag{19}$$

Here, x_i and x_j are the predicted molar compositions of the liquid phase in the flash calculation, and y_i and y_j are the predicted molar compositions of the vapor phase. In this work, the relative volatility is calculated between HFC-32 and HFC-125 in a given IL.

Step 8. Quantify uncertainty to inform experiments

Finally, we quantify how experimental measurement uncertainty impacts relative volatility and similar calculations. We utilize two different uncertainty quantification methods: Monte Carlo sampling and bootstrap re-sampling. Algorithm 1 describes our Monte Carlo approach, a standard method for uncertainty quantification and propagation.[86,87] The main idea is to simulate experimental uncertainty by adding normally distributed noise ϵ to the experimental composition. We choose to add this uncertainty to the compositions, as pressure and temperature are easier to control in laboratory experiments. We then resolve the flash calculation utilizing the newly regressed parameters and propagate this error to $\alpha_{i,j}$. Alternatively, we used `Parmest` bootstrap re-sampling of the data to quantify uncertainty. We eliminate two data points randomly, estimate the parameters, then re-sample and repeat the process to estimate the binary parameters. We draw 50 bootstrap samples from the data, with n-2 samples. For each instance of regressed parameters, the relative volatility

is computed. The key distinction between these approaches is that for Monte Carlo we must specify the measurement noise probability distribution; in contrast, with bootstrap, the measurement uncertainty is implicitly inferred from the data.

Algorithm 1 Monte Carlo Uncertainty Analysis

for $\epsilon = 1$–10% proportional to experimental composition **do**
  for *iteration* $= 1, 2, \ldots, 100$ **do**
    Add noise proportional to experimental composition, $x^{\epsilon}_{i,d} \leftarrow \mathcal{N}(x_{i,d}, x_{i,d} \cdot \epsilon)$
    Enforce composition bounds of 0 and 1
    Estimate parameters via Eq. (8) using $x^{\epsilon}_{i,d}$
    Perform flash calculation via Eq. (15) –(17)
    Calculate relative volatility via Eq. (19)
    Store results
  end for
  Calculate and store average volatility
  Calculate and store volatility standard deviation
end for
Plot the mean of the volatility and standard deviation vs. error %

Results

Peng-Robinson EoS accurately describes HFC/IL binary solubility data behavior

We begin our analysis by comparing the parameter regression results for the five postulated models. In Figure 2, we compare the predictions of solubility isotherms of HFC-32 and HFC-125 in [bmim][PF_6] as a function of composition computed using the regressed values for $\kappa_{i,j}$ with experimental binary solubility isotherm data. Table 2 shows the regressed parameters for the [bmim][PF_6] system. To assess the quality of fit, in Step 6, we utilize Eq. (18) to calculate the in-sample MAPE.

We first compare the models calibrated only using experimental binary solubility data (M_B, $M_{B,K}$). Figure 2(a) and 2(b) shows the pressure predictions of the models M_B and

Table 2: Binary interaction parameters for the five postulated models for HFC-32 or HFC-125 solubility in [bmim][PF_6].

Model	M_B	$M_{B,K}$	$M_{B,K}$	M_T	M_{BT}	$M_{BT,K}$	$M_{BT,K}$
Parameter	$\kappa_{Ai,j}$	$\kappa_{Ai,j}$	$\kappa_{Bi,j}$	$\kappa_{Ai,j}$	$\kappa_{Ai,j}$	$\kappa_{Ai,j}$	$\kappa_{Bi,j}$
i = **HFC-32**, j = **[bmim][PF_6]**	-0.0261	0.0270	-0.0488	-0.0435	-0.0328	-0.0248	-0.0056
i = **[bmim][PF_6]**, j = **HFC-32**	-0.0704	0.2680	-0.3153	-0.3506	-0.1131	-0.0106	-0.0910
i = **HFC-125**, j = **[bmim][PF_6]**	0.0589	-0.1114	0.1703	0.0604	0.0595	-0.1612	0.2123
i = **[bmim][PF_6]**, j = **HFC-125**	0.3454	-1.6016	2.0860	1.6779	0.4138	-1.7646	2.1235
i = **HFC-32**, j = **HFC-125**	0.0093	0.3926	-0.3891	0.0093	0.0093	0.3926	-0.3891
i = **HFC-125**, j = **HFC-32**	0.0074	-0.3754	0.3892	0.0074	0.0074	-0.3754	0.3892

$M_{B,K}$ compared to the experimental data. We observe that the fit is more accurate at lower concentrations of the HFCs. For HFC-32/[bmim][PF_6], we calculate an in-sample MAPE between predicted and experimental pressures of 7% for M_B and 5% for $M_{B,K}$. We also observe that for HFC-125/[bmim][PF_6], the fit is considerably better for $M_{B,K}$ at 7% MAPE, as it accounts for temperature dependency for binary parameters, compared to a MAPE of 15% for M_B. We find the binary parameters are more dependent on temperature in the HFC-125/[bmim][PF_6] system than HFC-32/[bmim][PF_6] system. We hypothesize that temperature dependence is necessary because of the concave shape of the HFC-125 isotherm. We emphasize that the temperature dependence shown in Eq. (7) can only be regressed with data sets that contain measurements at two or more temperatures.

Next, we compare the models that are calibrated using only experimental ternary solubility data (M_T) and both experimental binary and ternary solubilty data (M_{BT}, $M_{BT,K}$). Figure 2(c) and 2(d) shows that model M_T, calibrated only with experimental ternary solubility data has an out-of-sample MAPE of at least 30% when predicting solubility for binary HFC/IL systems. This is explained by two different features of the experimental ternary solubility data set. The first is that the data set contains only two binary HFC/IL data points for each HFC, one at each of the two experimental pressures. In other words, the experimental ternary solubility data set includes an HFC-32/IL data point at 0.1 MPa and an HFC-32/IL data point at 0.25 MPa, as well as two data points at the same pressures for HFC-125. Second, the availability of this experimental data at only two pressures and one temperature (298 K) necessitates extrapolation to higher pressures and different tempera-

tures.

We calculate the in-sample MAPE between predicted and experimental pressures for HFC-32/[bmim][PF_6] as 7.5% for M_{BT} and 5.2% for $M_{BT,K}$. For HFC-125/[bmim][PF_6] the in-sample MAPE is 15.8% for M_{BT} and 7.4% for $M_{BT,K}$. We note that in-sample MAPE of the predicted pressure of M_B versus M_{BT} and $M_{B,K}$ versus $M_{BT,K}$ are almost identical, which is attributed to the exclusion or inclusion of temperature-dependent binary parameters. We can also observe from Table 2 the order of magnitude change in $\kappa_{Ai,j}$. M_{BT} and $M_{BT,K}$, calibrated with binary and ternary data, estimate binary solubility with higher accuracy than M_T, as the addition of binary data reduces the interpolation problem of M_T. None of the calibrated models using only ternary data or a combination of binary and ternary data, M_T, M_{BT}, and $M_{BT,K}$, have a significantly lower in-sample MAPE than M_B and $M_{B,K}$, the models calibrated only with experimental binary solubility data.

EoS parameterized with binary or ternary data give accurate phase equilibrium predictions

Figure 3 compares ternary solubility predictions for models M_B to $M_{BT,K}$ against experimental ternary solubility of HFC-32/HFC-125/[bmim][PF_6] in a ternary phase diagram (Step 4) using the regressed parameters in Table 2. We calculate the vapor and liquid phase compositions with Eqs. (1) to (10) at 298 K and 1 MPa and compositions of the ternary mixture extracted from the ternary data set.

As expected, we find that the predictions utilizing M_T, which has no κ temperature dependence and was calibrated only with experimental ternary data, has a 1% in-sample MAPE. In contrast, we find that the predictions of M_B and $M_{B,K}$ (both models only calibrated with experimental binary solubility data) have an out-of-sample MAPE of 10.1% and 10.2%, compared to the ternary experimental compositions in Baca *et al.*[60] The error is consistent with the difference observed between the data sets in Figure 3. We emphasize these measurements we obtained with different experimental methods and equipment (as

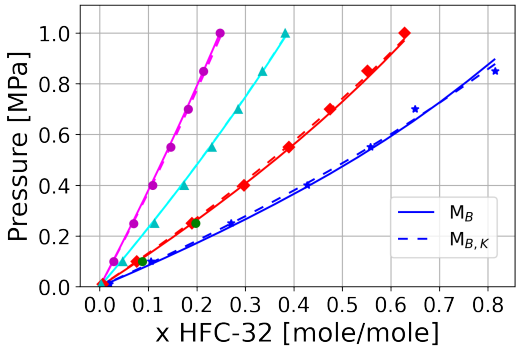

(a) Isotherms for HFC-32 solubility in [bmim][PF_6] predicted with M_B and $M_{B,K}$

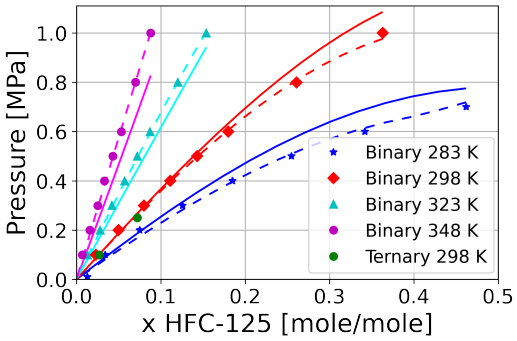

(b) Isotherms for HFC-125 solubility in [bmim][PF_6] predicted with M_B and $M_{B,K}$

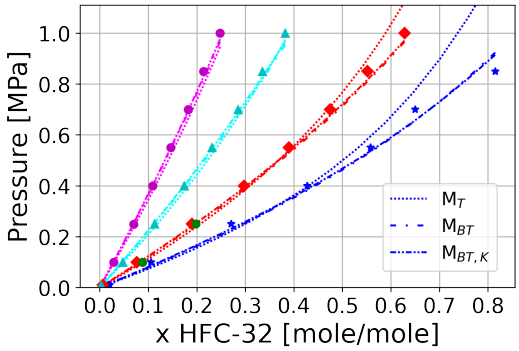

(c) Isotherms for HFC-32 solubility in [bmim][PF_6] predicted with M_T, M_{BT} and $M_{BT,K}$

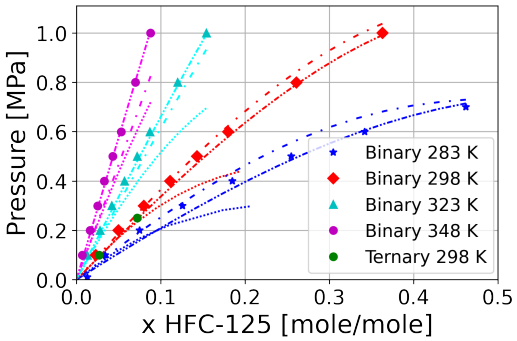

(d) Isotherms for HFC-125 solubility in [bmim][PF_6] predicted with M_T, M_{BT} and $M_{BT,K}$

Figure 2: Comparison of experimental solubility isotherms (points) and solubility predictions (dashed lines) made with models M_B (κ temperature dependence, fitted to experimental binary data[18]), $M_{B,K}$ (κ temperature dependence, fitted to experimental binary data[18]), M_T (no κ temperature dependence, fitted to experimental ternary data[29]), M_{BT} (no κ temperature dependence, fitted to both experimental binary[18] and ternary data[29]) and $M_{BT,K}$ (κ temperature dependence, fitted to both experimental binary[18] and ternary data[29]).

described in the references), so a modest difference is to be expected.

Predictions made with models M_{BT} and $M_{BT,K}$ (models calibrated from both data sets) have an in-sample MAPE of 9.5% and 9.2%, respectively. The predictions are qualitatively consistent between models calibrated from experimental binary or ternary solubility data sets. The findings give us confidence in the EoS and provide a benchmark to compare the results of the binary prediction (see below). This significant result allows us to compare different IL behavior qualitatively as the ternary data now acts as an out-of-sample validation

for the binary models M_B and $M_{B,K}$.

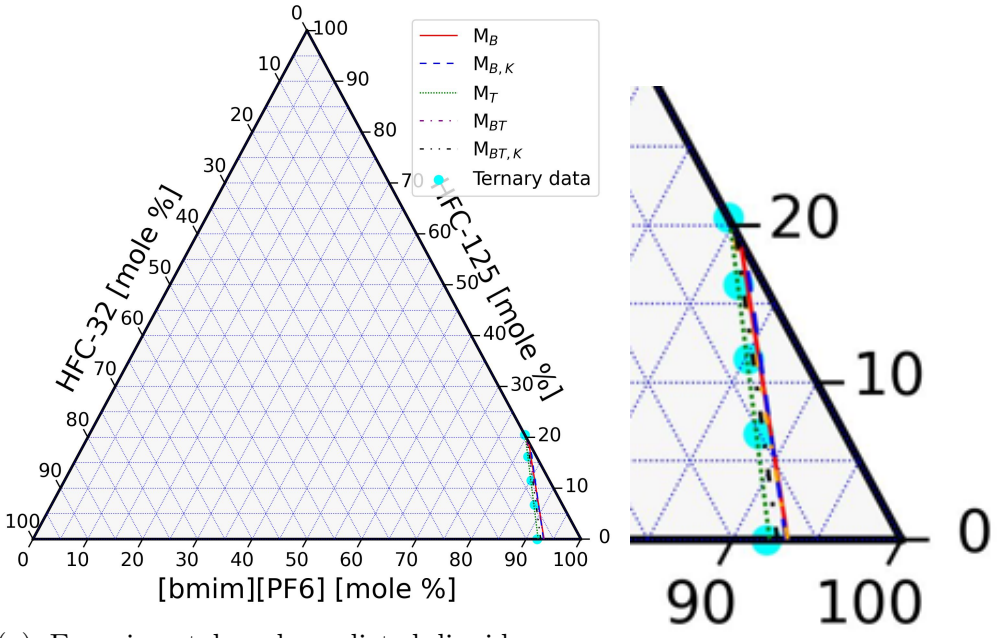

(a) Experimental and predicted liquid compositions for HFC-32/HFC-125/[bmim][PF_6] calculated utilizing M_B, $M_{B,K}$, M_T, M_{BT} and $M_{BT,K}$.

(b) A zoomed in look at the ternary composition results.

Figure 3: Ternary diagram liquid compositions calculated from two different data sets. M_B, $M_{B,K}$ were calibrated with binary data.

Similarly, Figure 4 shows the absorption of each HFC and the total absorption to the IL phase. We first note that the difference between the absorption predicted in both experimental data sets is consistent with the differences shown in Figure 2, i.e., the data sets have a better agreement with respect to HFC-32 than HFC-125. M_B prediction is consistent with the binary data with a MAPE of 2.7%. However, $M_{B,K}$ prediction has a MAPE of 1% compared to the binary experimental data, consistent with the finding in the pressure prediction shown in Figure 2, as it accounts for the temperature dependency.

M_T gives an accurate prediction compared to the ternary experimental data, as it was calibrated with this data. In comparison, M_{BT} predicts approximately the average of the two data sets. We note how weighing the ternary data changes the behavior of the temperature dependence. $M_{B,K}$ predicted less absorption of HFC-32 than M_B while, $M_{BT,K}$ considers more absorption of HFC-32 than M_{BT}. This is explained by the addition in the weighted

parameterization of the ternary data set, which contains more data at low pressures and 298 K. Although M_T predictions show the lower MAPE with respect to absorption, we caution against the use of the model at higher pressures: as shown in Figure 2(c) and 2(d), M_T does not have a good quality of fit at high pressures as it was only calibrated at a maximum of 0.25 MPa and 298 K.

Binary data and PR EoS models are sufficiently accurate to perform early process design and relative volatility estimation

We now quantify how the differences between the models M_B through $M_{BT,K}$ impact process design and IL screening calculations. We calculate a flash unit from Shiflett *et al.*[13] described in the Methods (Step 5), which is a proxy for the overall separation process design. In Figure 5, we systematically vary the outlet temperature from 280 K to 325 K to compare the predicted HFC-32 vapor recovery fraction. From the results, we observe a 4% to 20% difference between the vapor recovery fraction predictions from the models at low temperatures. The difference in models is consistent with Figure 4. M_B and $M_{B,K}$ show a maximum discrepancy of 10% of the vapor recovery fraction. Additionally, M_{BT} and $M_{BT,K}$ reconcile the models calibrated with binary data and M_T. The models that show the highest difference in predicted HFC-32 vapor recovery (20%) are $M_{B,K}$ and M_T. We also note that the flash vapor is enriched in HFC-32 (above 98 mol%), at which, as seen in Figures 2(a) and 2(c), M_T solubility predictions show a MAPE of only 5%. However, as shown in Figure 2(d), M_T should be used with caution when calculating equilibrium at pressures above 0.25 MPa and temperatures different than 298 K and in mixtures with concentrations of HFC-125 above 10 mol%. The fact that any of the models can qualitatively predict the vapor recovery fraction of the flash calculation shows that we can perform early process design with our models and one or both data sets. If multiple unique data sets are available, i.e., both binary and ternary solubility data, we recommend using the EoS model calibrated with the most data for process design. Leave-one-out (i.e., jackknife resampling) analysis can be

used to estimate the out-of-sample prediction uncertainty which can be propagated through the process design analysis (as described below).

To determine if the qualitative results translate to relative volatility, we calculate the phase equilibrium of a 0 mol% HFC-125, 70 mol% HFC-32, and 30 mol% of [bmim][PF_6] mixture. We then increased the concentration of HFC-125 by 5 mol% and reduced the HFC-32 by the same amount until 70 mol% of HFC-125 had been reached and recalculated the relative volatility. We do this for all the models and plot the results in Figure 6. We observe the same qualitative trend of 2.8 to 3.4 relative volatility consistent across all the models, as the flash calculation results shown in Figure 5. We note the experimental relative volatility was calculated with ternary data and, as a consequence, M_T gives the best relative volatility prediction because it was calibrated with the same ternary data. However, these results suggest that M_B, the simplest model, is sufficient for ranking ILs as candidate entrainers.

The framework evaluates candidate IL entrainers in minutes

Ultimately, we envision using this framework to facilitate data-driven IL entrainer screening and selection (Step 7). To demonstrate this, we calculate the relative volatility of HFC-125 with respect to HFC-32 in six different ILs at varying liquid concentrations of HFC-125, shown in Figure 7(a). Visually, the relative volatility metric does not seem to vary with HFC-125 liquid composition. However, there is a 5% decrease in volatility as the HFC-125 liquid mole fraction increases, which is consistent across all of the six ILs studied. This result is on the same order of magnitude as findings from Li *et al.*[34] which showed that with a 30 mol% IL feed, relative volatility decreased by approximately 14% as the composition of the other mixture component changed. We hypothesize this small change in volatility as liquid HFC composition changes results from weak molecular-level interactions between HFCs in the liquid phase, i.e., if there were more interactions between the liquid phase HFCs, there would be more significant relative volatility variations. This suggests that in the search for an IL entrainer, the focus should be given to ILs which interact more strongly with HFCs

to prevent further HFC interactions. For IL screening, these results show that evaluating the relative volatility metric at a single composition is sufficient. These results guide us to select [bmim][PF_6] as the entrainer for separating R-410A from the set of ILs in this study. We note that even though the relative volatility is an essential factor in an HFC separation process, it is necessary to model other properties, such as the density, viscosity, and heat capacity of the ILs so that their impact on the economics of the process can be analyzed.

We profile computational times of the workflow using a Windows PC with Intel(R) Core(TM) i7-7500U CPU with 2.90 GHz and 16 GB of RAM. Overall, implementing the entire workflow to screen a single IL takes between 7 and 25 minutes, depending on the amount of available data and the thermodynamic model. The time requirements of Steps 1 and 2 is negligible. In Step 3, thermodynamic model parameter estimation, for a data set containing six data points (e.g., [bmim][Ac], [hmim][FAP], [hmim][Cl]), parameterization took two minutes, while for a data set containing sixty data points (e.g., [bmim][PF_6]), parameterization took twenty minutes. (The optimal parameters for each HFC/IL dataset are reported in Table 3). We believe there are opportunities to optimize the model initialization in IDAES-PSE and `parmest` to reduce this time significantly. Steps 4, 5, and 7, which are necessary for performing the relative volatility and screening analysis, took on average five minutes to complete. Thus, Step 3 is the most computationally demanding step of the workflow. We emphasize that this framework can be used for entrainer screening via other metrics, such as ternary diagram evaluation or selectivity analysis because phase equilibrium (Steps 4 and 5) can be computed in minutes. In total, we applied the complete framework to the six ILs in two hours, analyzing each IL sequentially. However, we note that the calculations in this workflow, which are independent for each IL, would be trivial to parallelize with multiple CPU cores or computers.

Table 3: Binary interaction parameters for model M_B for HFC-32 or HFC-125 solubility in various ILs.

IL	Model	Parameter	HFC-32/IL	IL/HFC-32	HFC-125/IL	IL/HFC-125	HFC-32/HFC-125	HFC-125/HFC-32
[bmim][BF_4]	M_B	$\kappa_{Ai,j}$	-0.0068	-0.0282	0.0645	0.5715	0.0093	0.0074
[bmim][Ac]	M_B	$\kappa_{Ai,j}$	-0.0254	-0.0313	-0.0214	-0.1105	0.0093	0.0074
[emim][Tf_2N]	M_B	$\kappa_{Ai,j}$	-0.0261	-0.0704	-0.0215	-0.1106	0.0093	0.0074
[hmim][Cl]	M_B	$\kappa_{Ai,j}$	0.0271	-0.2974	-0.0469	-0.0550	0.0093	0.0074
[hmim][FAP]	M_B	$\kappa_{Ai,j}$	-0.0254	-0.0155	-0.0418	-0.1354	0.0093	0.0074

What experimental precision is adequate for IL screening?

To aid experimental design we estimate how measurement uncertainty impacts relative volatility calculations by applying the Monte Carlo and bootstrap algorithms (Step 8). In Figure 7(b), we plot the mean of the volatility calculated using M_B and the standard deviation versus the percentage of experimental error. Table 3 presents the mean and standard deviation of the regressed parameters, which are consistent using both uncertainty quantification techniques.

From Figure 7(b) and Table 3, we observe that a 5% error in experimental measurements translates 5% deviation in relative volatility. We also observe that the standard deviation is higher in systems where the volatility is higher and where data at different temperatures is available, as is the case for [bmim][PF_6] and [bmim][BF_4]. We observe that the error bars induced are more significant than the change in volatility compared to Figure 7(a). We note that the experimental precision required depends on the closeness of the volatilities of the mixtures and the type of data from which the parameters are fitted. In the case of the ILs being compared in this study, only error values above 8% to 9% (when the error bars overlap) could change the decision from [bmim][PF_6] to [bmim][BF_4]. Recall, each error bar corresponds to one standard deviation in the relative volatility estimate. Thus the probability of experimental errors at the upper extreme for one IL candidate, e.g., [bmin][PF_6], and lower extreme for another, e.g., [bmin][BF_4], is low. Based on the results for these two ILs, we conclude a 10% experimental precision is adequate to rank ILs with a relative volatility difference of 0.3 ($\approx 3.03 - 2.74$ at 50 mol% HFC-125) based on Fig. 7(a). To our knowledge, this is one of the first studies to recommend a quantitative threshold

for acceptable experimental error based on process metrics such as relative volatility for IL screening.

Table 4: Uncertainty in binary interaction parameters for model Mone for HFC-32 or HFC-125 solubility in [bmim][PF_6].

Model	**Stat**	$\mathbf{M}_B$ 1% error	$\mathbf{M}_B$ 2% error	$\mathbf{M}_B$ 5% error	$\mathbf{M}_B$ 9% error	$\mathbf{M}_B$ 10% error	$\mathbf{M}_B$ bootstrap
HFC-32/[bmim][PF_6]	mean	-0.0272	-0.0274	-0.0276	-0.0276	-0.0276	-0.0271
HFC-32/[bmim][PF_6]	standard deviation	0.0001	0.0004	0.0004	0.0006	0.0006	0.0022
[bmim][PF_6]/HFC-32	mean	-0.0781	-0.0757	-0.0751	-0.0724	-0.0724	-0.0886
[bmim][PF_6]/HFC-32	standard deviation	0.0007	0.0071	0.0139	0.0200	0.0201	0.0391
HFC-125/[bmim][PF_6]	mean	0.0584	0.0579	0.0534	0.0468	0.0470	0.0636
HFC-125/[bmim][PF_6]	standard deviation	0.0014	0.0019	0.0034	0.0043	0.0050	0.0074
[bmim][PF_6]/HFC-125	mean	0.3367	0.3331	0.3365	0.3320	0.3348	0.4941
[bmim][PF_6]/HFC-125	standard deviation	0.0163	0.0276	0.2338	0.2397	0.2440	0.2065

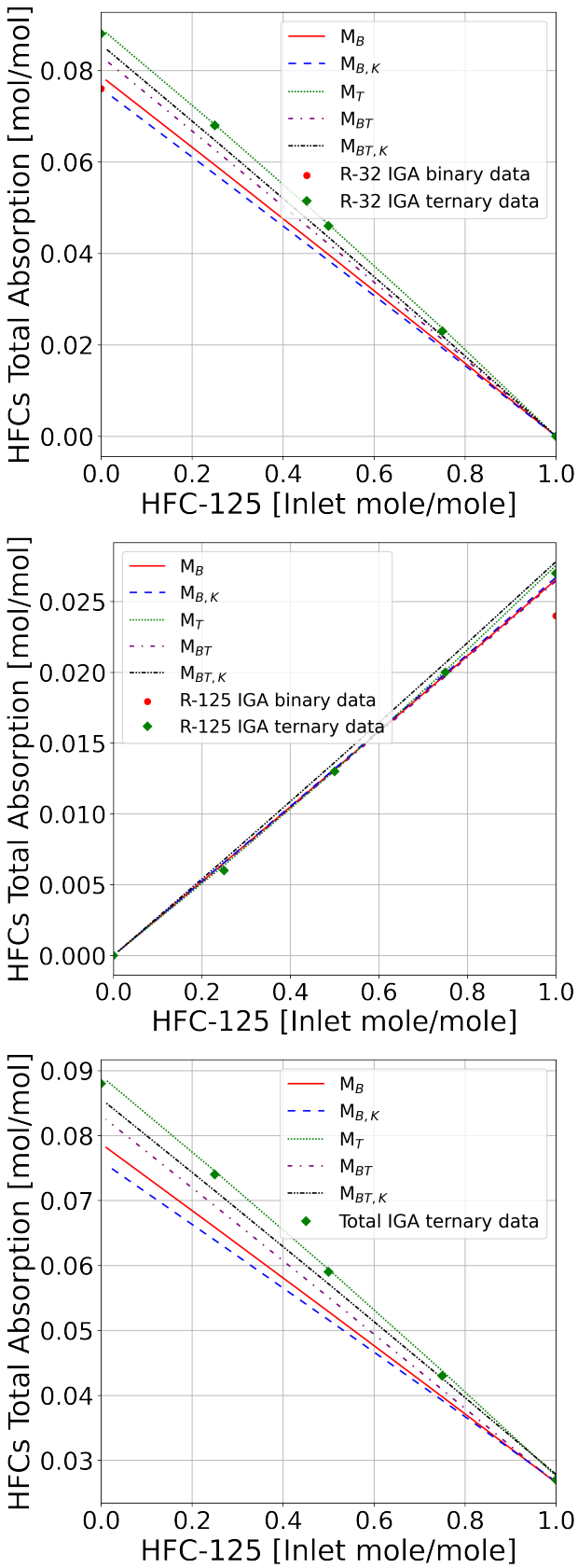

Figure 4: Predicted HFC-32/HFC-125/[bmim][PF_6] ternary absorption compared to experimental data from Baca *et al.*[29] M_B and $M_{B,K}$ were only calibrated with experimental binary solubility data. M_T was calibrated with only with experimental ternary solubility data. M_{BT} and $M_{BT,K}$ where calibrated with both experimental binary and ternary solubility data.

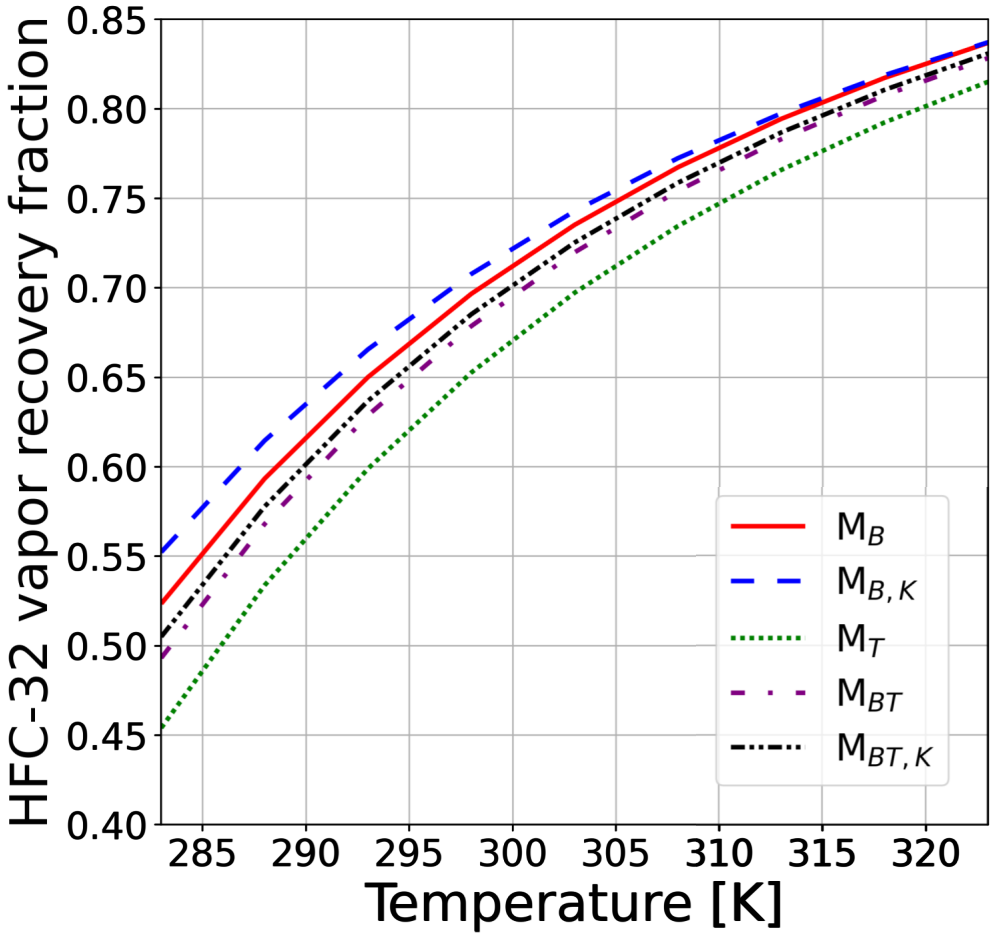

Figure 5: HFC-32 vapor phase recovery from [bmim][PF_6] versus temperature predicted with models M_B to $M_{BT,K}$.

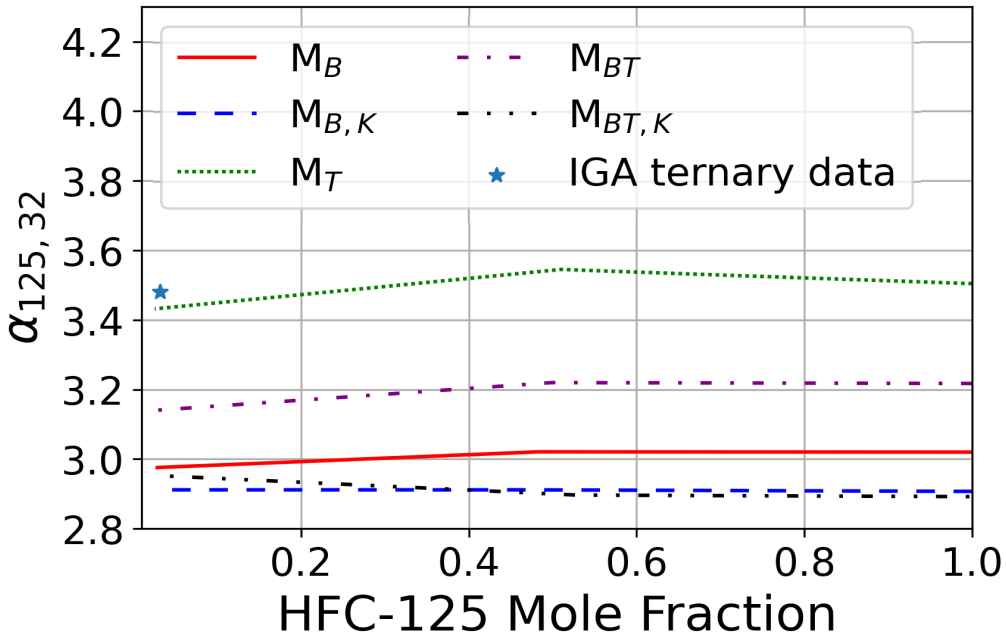

Figure 6: Relative volatility predictions for HFC-32 and HFC-125 in [bmim][PF_6] calculated with models M_B to $M_{BT,K}$.

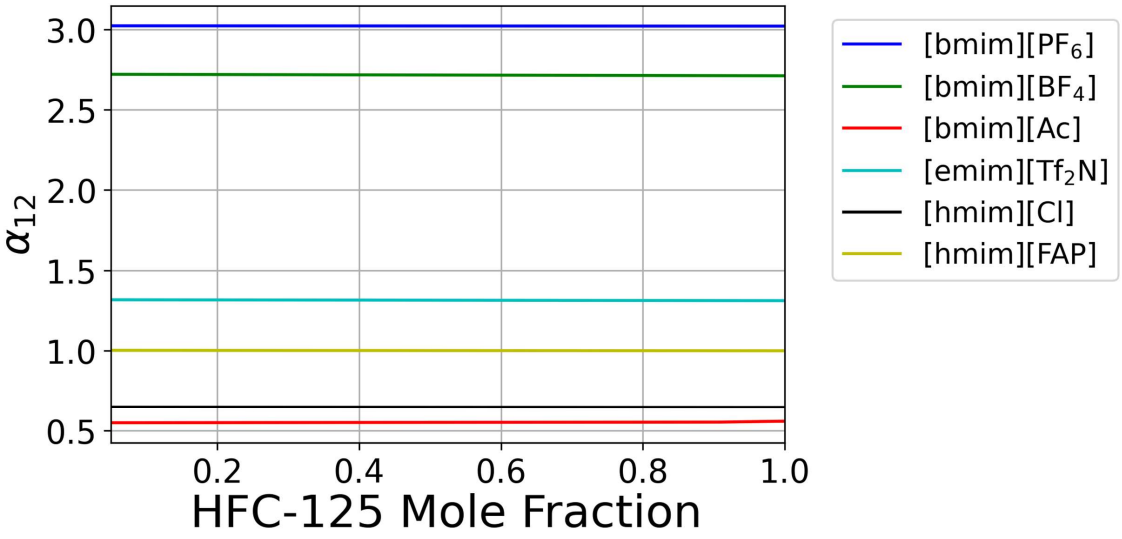

(a) Relative volatility calculate with experimental binary solubility data for HFC-32 and HFC-125 in six ILs.

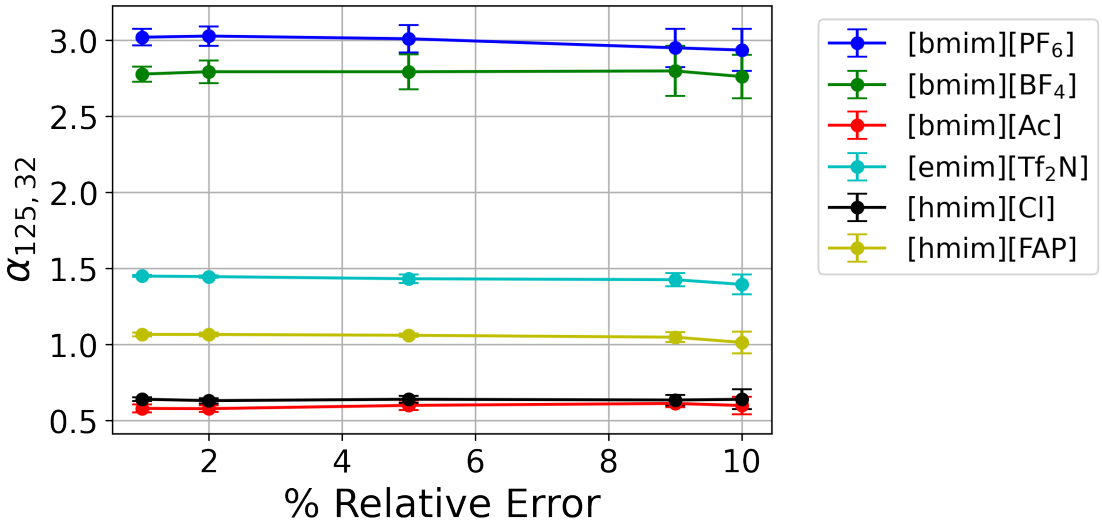

(b) Mean of the relative volatility versus relative error of the experimental data. Error bars are the standard deviation of the relative volatility.

Figure 7: Comparing the relative volatility of HFC-32 and HFC-125 in different ILs provides a qualitative reason for understanding which ILs may be optimal entrainers.

Conclusions and Future Work

We developed a data analysis toolkit, built upon the open-sourced IDAES-PSE framework and Pyomo ecosystem, to calculate the VLE of HFC and IL mixtures and then rapidly screen IL entrainers. The approach calibrates PR EoS binary interaction parameters to binary and first-of-their-kind ternary HFC and IL mixture data. We harness the fitted EoS to study phase predictions, flash calculations, and in-sample and out-of-sample error metrics. Next, relative volatility of HFCs is computed for IL screening. Finally, Monte Carlo and bootstrap methods are used to quantify and propagate uncertainty in the data and EoS models through process design calculations and to inform experimental design. We applied this framework to screen six ILs ([bmim][PF_6], [bmim][BF_4], [emim][Tf_2N], [bmim][Ac], [hmim][FAP], [hmim][Cl]) and found that [bmim][PF_6] is the ideal entrainer for HFC-32/HFC-125, which comprise the refrigerant R-410a, separations. This workflow can be implemented in minutes to hours to rapidly assess up to hundreds of IL entrainers, if data is available. We emphasize that the proposed framework is flexible and can be easily extended to consider additional thermophysical properties such as density, viscosity, and heat capacity, and other environmentally important systems in need of rapid evaluation techniques, such as CO_2 capture and biomass energy sources (tert-butanol/ethanol/water mixtures).

Using the proposed framework, we gained several insights regarding the search for IL entrainers to facilitate separations of HFC refrigerants for their reuse and recycle. We found that experimental binary HFC/IL solubility measurements taken at multiple temperatures are more valuable than the new ternary HFC/IL mixture measurements conducted at a single temperature. The reason for this is two-fold: a) accurate phase predictions, flash calculations, and ternary mixture predictions can be made using PR EoS models parameterized with binary solubility data; and b) the binary interaction parameters are influenced by temperature, indicating the need for data measured at a range of temperatures. Additionally, we show that binary data is sufficient to show qualitative results for IL entrainer screening and preliminary process design. Finally, we found that for a given IL, the relative volatility

between the two HFCs studied remains relatively constant as the HFC composition within the mixture changes. This implies that that qualitative screening of ILs can be rapidly accomplished via straightforward relative volatility calculations at a single HFC/IL mixture composition. Our results show that these IL screening decisions can be made with up to ten percent error in a given data sets.

Thus, moving forward, we recommend a multistage IL screening approach. First, relative volatility of HFCs in many ILs should be measured at a single composition to facilitate initial IL screening and down-selection. Second, binary HFC/IL data at multiple temperatures should be gathered for the most promising ILs. Third, using this data, thermodynamic and process modeling calculations with uncertainty analysis should be performed. Fourth, for the best IL entrainer separation systems, sparse ternary mixture measurements should be made to validate liquid phase predictions. Thus, for IL screening, emphasis should be placed on gathering a variety of data over experimental accuracy. While not essential for preliminary HFC separation process design and IL entrainer screening, ternary data is useful in the further validation and refinement of predictions made with models parameterized with binary data and can provide additional enrichment of a data set. Furthermore, we found several opportunities of utilizing model based design of experiments (MBDoE)[88] to inform the minimum required dataset for screening at each step of the framework. Finally, a SAFT-based[61,79] or machine learning method[89] may be implemented to predict ILs for HFC separations.

We note that our recommendations are pragmatically engineering focused and may be at odds with current practices of gathering full isotherm data for each HFC/IL mixture before considering process scale implications. Hence, this work highlights a possible tension between scientific goals, e.g., understanding mechanisms and publishing full HFC/IL solubility isotherms, and engineering needs. Our intention with these findings is to guide both laboratory and molecular simulation data generation efforts, which have been focusing in recent years more on studying ILs at a single temperature and creating new tools to gather increas-

ingly complex data (e.g., ternary mixture measurements), by understanding what data are sufficient for molecular and process design decisions. Within this context, there are several outstanding research questions which can be addressed in the future with extensions of our proposed framework: a) Which thermodynamic model is best in terms of fit and simplicity for a given HFC/IL mixture? b) How can process simulation and optimization be used to manage trade-offs between predictive accuracy for multiple properties, e.g., partition coefficient, viscosity, in the context of multi-fidelity experimental (or simulation) screening? c) Are alternate parameter temperature dependencies (beyond linear) supported by the data? d) How do properties other than relative volatility and phase equilibrium, such as density, viscosity, and heat capacity, affect the cost of an HFC separation process? e) How does uncertainty impact the optimal flowsheet configuration and detailed process design for each HFC/IL system? More broadly, these open questions are pertinent to practically all green solvent design applications.

Nomenclature

Sets and Elements

$\mathcal{C}$	Components
D	Data sets
$\mathcal{O}$	Outlet streams

Indices

$i, j \in \mathcal{C}$	Component
$d \in D$	Data set
in	Inlet stream
$l \in \mathcal{O}$	Outlet streams
liq	Liquid phase
vap	Vapor phase

Variables

$\alpha_{i,j}$	Volatility of component i relative to component j
a_m	a unlike-interaction parameter
b_m	b unlike-interaction parameter
F	Flow (mol/s)
P	Pressure (MPa)
$\Phi_{phase,i}$	Fugacity of component i
T	Temperature (K)
T_1	Intermediate temperature variable (K)
T_{bubble}	Bubble temperature (K)
T_{eq}	Equilibrium temperature (K)
T_{dew}	Dew temperature (K)
$\hat{P}$	Calculated obtained pressure (MPa)
V	Volume
x	Liquid molar composition
y	Vapor molar composition

Parameters

a	Attraction between molecules
b	Volume occupied by molecules
ϵ_1	Smoothing parameter 1
ϵ_2	Smoothing parameter 2
κ	Binary interaction parameter
P_c	Critical pressure (MPa)
R	Ideal gas constant
T_c	Critical temperature (K)

Abbreviations

EoS	Equation of State
EPA	Enviromental Protection Agency
GWP	Global Warming Potential
HFC	Hydrofluorocarbon
IDAES	Institute for the Design of Advanced Energy Systems
IL	Ionic Liquid
MAPE	Mean absolute percentage error
VLE	Vapor-Liquid Equilibrium

Acknowledgements

This work was funded by the U.S. National Science Foundation under grant CBET-1917474. B.J.B. graciously acknowledges support from the Richard and Peggy Notebaert Premier Fellowship at the University of Notre Dame. A.W.D., A.G., and M.M. thank the University of Notre Dame for additional financial support.

We thank Prof. Edward J. Maginn at the University of Notre Dame for insightful conversations regarding thermodynamic modeling and the need for process scale feedback to inform experiments and molecular simulations. Likewise, we thank Prof. Mark Shiflett and Kalin Baca at the University of Kansas for contributing to discussions regarding the binary and ternary solubility mixture data.

CRediT Author Statement

A.G.: Conceptualization, Methodology (Lead), Software (Lead), Visualization, Data Curation, Formal Analysis, Writing; **B.J.B.**: Conceptualization, Methodology, Software, Visualization, Data Curation, Formal Analysis, Writing; **G.F.**: Data Curation, Software, Formal Analysis; **M.M.**: Literature Review, Data Curation; **A.W.D.**: Conceptualization, Method-

ology, Writing, Supervision, Project Administration, Funding Acquisition.

References

(1) Ko, M.; Shia, R.; Sze., N.; Magid, H.; Bray, R. G. Atmospheric lifetime and global warming potential of HFC-245fa. *Journal of Geophysical Research* **1999**, *104*, 8173–8181.

(2) Clerbaux, C.; R.,; Colin, P. C. S.; ; Granier, C. Infrared Cross Sections and Global Warming Potentials of 10 Alternative Hydrohalocarbon. *Journal Of Geophysical Research* **1993**, *98*, 10,491–10,497.

(3) Xu, Y.; Zaelke, D.; Velders, G. J. M.; Ramanathan, V. The role of HFCs in mitigating 21st century climate change. *Atmospheric Chemistry and Physics* **2013**, *13*, 6083–6089.

(4) EPA, Greenhouse Gas Inventory Data Explorer. Date of Access: 04/07/2022; https://cfpub.epa.gov/ghgdata/inventoryexplorer/#allsectors/allsectors/fluorinatedgases/gas/all.

(5) UN, Amendment To The Montreal Protocol On Substances That Deplete The Ozone Layer. Date of Access: 04/07/2022; https://treaties.un.org/doc/Publication/CN/2016/CN.872.2016-Eng.pdfl.

(6) EPA, Phasedown of Hydrofluorocarbons: Establishing the Allowance Allocation and Trading Program Under the American Innovation and Manufacturing Act. Date of Access: 04/07/2022; https://www.epa.gov/climate-hfcs-reduction/final-rule-phasedown-hydrofluorocarbons-establishing-allowance-allocation.

(7) EPA, Draft Regulatory Impact Analysis for Phasing Down Production and Consumption of Hydrofluorocarbons HFCs. Date of Access: 04/07/2022; https://www.epa.gov/sites/default/files/2021-05/documents/ria_omb_043021_0.pdf.

(8) Daikin, 32 Reasons why R-32 is the right answer. Date of Access: 04/07/2022; https://www.r32reasons.com/resources.

(9) Daikin, R-32: The Most Balanced Refrigerant for Stationary Air Conditioners and Heat Pumps. Date of Access: 4/07/2022; https://www.daikin.com/csr/information/influence/hfc32.

(10) Brown, J. S. HFOs New, Low Global Warming Potential Refrigerants. *ASHRAE Journal* **2009**, *51*, 22–29.

(11) Lei, Z.; Li, C.; Chen, B. Extractive Distillation: A Review. *Separation & Purification Reviews* **2003**, *32*, 121–213.

(12) Lei, Z.; Chen, B.; Ding, Z. *Special Distillation Processes*; Elsevier Science: Amsterdam, 2005; pp 145–177.

(13) Shiflett, M.; Yokozeki, A. Separation of difluoromethane and pentafluoroethane by extractive distillation using ionic liquid. *Chimica Oggi-chemistry Today* **2006**, *24*, 28–30.

(14) Liu, X.; He, M.; Lv, N.; Qi, X.; Su, C. Solubilities of R-161 and R-143a in 1-Hexyl-3-methylimidazolium bis(trifluoromethylsulfonyl)imide. *Fluid Phase Equilibria* **2015**, *388*, 37–42.

(15) Liu, X.; He, M.; Lv, N.; Qi, X.; Su, C. Vapor–Liquid Equilibrium of Three Hydrofluorocarbons with [HMIM][Tf2N]. *Journal of Chemical & Engineering Data* **2015**, *60*, 1354–1361.

(16) Liu, X.; Qi, X.; Lv, N.; He, M. Gaseous absorption of fluorinated ethanes by ionic liquids. *Fluid Phase Equilibria* **2015**, *405*, 1–6.

(17) Shiflett, M. B.; Harmer, M. A.; Junk, C. P.; Yokozeki, A. Solubility and diffusivity

of 1,1,1,2-tetrafluoroethane in room-temperature ionic liquids. *Fluid Phase Equilibria* **2006**, *242*, 220–232.

(18) Shiflett, M. B.; Harmer, M. A.; Junk, C. P.; Yokozeki, A. Solubility and Diffusivity of Difluoromethane in Room-Temperature Ionic Liquids. *Journal of Chemical & Engineering Data* **2006**, *51*, 483–495.

(19) Shiflett, M. B.; Yokozeki, A. Solubility Differences of Halocarbon Isomers in Ionic Liquid [emim][Tf2N]. *Journal of Chemical & Engineering Data* **2007**, *52*, 2007–2015.

(20) Shiflett, M. B.; Yokozeki, A. Binary Vapor–Liquid and Vapor–Liquid–Liquid Equilibria of Hydrofluorocarbons (HFC-125 and HFC-143a) and Hydrofluoroethers (HFC-125 and HFC-143a) with Ionic Liquid [emim][Tf2N]. *Journal of Chemical & Engineering Data* **2008**, *53*, 492–497.

(21) Separation of tetrafluoroethylene and carbon dioxide using ionic liquids. *Separation and Purification Technology* **2011**, *79*, 357–364.

(22) Yokozeki, A.; Shiflett, M. B. Global phase behaviors of trifluoromethane in ionic liquid [bmim][PF6]. *AIChE Journal* **2006**, *52*, 3952–3957.

(23) Yokozeki, A.; Shiflett, M. B. Vapor–liquid equilibria of ammonia+ionic liquid mixtures. *Applied Energy* **2007**, *84*, 1258–1273.

(24) Yokozeki, A.; Shiflett, M. B. Separation of Carbon Dioxide and Sulfur Dioxide Gases Using Room-Temperature Ionic Liquid [hmim][Tf2N]. *Energy & Fuels* **2009**, *23*, 4701–4708.

(25) Finberg, E. A.; Shiflett, M. B. Process Designs for Separating R-410A, R-404A, and R-407C Using Extractive Distillation and Ionic Liquid Entrainers. *Industrial & Engineering Chemistry Research* **2021**, *60*, 16054–16067.

(26) Monjur, M. S.; Iftakher, A.; Hasan, M. M. F. Separation Process Synthesis for High-GWP Refrigerant Mixtures: Extractive Distillation using Ionic Liquids. *Industrial & Engineering Chemistry Research* **2022**, *61*, 4390–4406.

(27) Garciadiego, A.; Mazumder, M.; Befort, B. J.; Dowling, A. W. *Computer Aided Chemical Engineering*; Elsevier, 2022; Vol. 49; pp 307–312.

(28) Plechkova, N. V.; Seddon, K. R. Applications of ionic liquids in the chemical industry. *Chemical Society Reviews* **2008**, *37*, 123–150.

(29) Baca, K. R.; Broom, M. G. R., Darren P.; Benham, M. J.; Shiflett, M. B. First measurements for the simultaneous sorption of Difluoromethane and Pentafluoroethane mixtures in ionic liquids using the Integral Mass Balance method. *Industrial & Engineering Chemistry Research* **2022**, *61*, 9774–9784.

(30) McKetta, J. J. *Unit Operations Handbook*; CRC Press, 1992.

(31) Prokopakis, G. J.; Seider, W. D. Feasible specifications in azeotropic distillation. *AIChE Journal* **1983**, *29*, 49–60.

(32) Berg, L. Azeotropic and extractive distillation: Selecting the agent for distillation. *Chemical Engineering Progress* **1969**, *65*, 52–57.

(33) Pham, H. N.; Doherty, M. F. Design and synthesis of heterogeneous azeotropic distillations—II. Residue curve maps. *Chemical Engineering Science* **1990**, *45*, 1837–1843.

(34) Li, Q.; Zhang, J.; Lei, Z.; Zhu, J.; Zhu, J.; Huang, X. Selection of Ionic Liquids as Entrainers for the Separation of Ethyl Acetate and Ethanol. *Industrial & Engineering Chemistry Research* **2009**, *48*, 9006–9012.

(35) Cho, J.; Jeon, J. Optimization Study on the Azeotropic Distillation Process for Isopropyl Alcohol Dehydration. *Korean Journal of Chemical Engineering* **2006**, 1–7.

(36) Rodríguez-Donis, I.; Gerbaud, V.; Joulia, X. Entrainer Selection Rules for the Separation of Azeotropic and Close-Boiling-Temperature Mixtures by Homogeneous Batch Distillation Process. *Industrial & Engineering Chemistry Research* **2001**, *40*, 2729–2741.

(37) Webb, W. Industrial Alcohol. *Chemical Engineering Research and Design* **1937**, *15*, 243–252.

(38) Guinot, F., H. & Clark Azeotropic distillation in industry. *Chemical Engineering Research and Design* **1938**, *16*, 189–199.

(39) Ramírez-Corona, N.; Schramm-Flores, A.; Reyes-Lombardo, S. Effect of ionic liquids as entrainers on the dynamic behavior of ethanol-water extractive columns. *BMC Chemical Engineering* **2019**, *1*, 23.

(40) Figueroa, J.; Lunelli, B. H.; Filho, R. M.; Maciel, M. W. Improvements on Anhydrous Ethanol Production by Extractive Distillation using Ionic Liquid as Solvent. *Procedia Engineering* **2012**, *42*, 1016–1026.

(41) Marsh, K.; Boxall, J.; Lichtenthaler, R. Room temperature ionic liquids and their mixtures—a review. *Fluid Phase Equilibria* **2004**, *219*, 93–98, Molecular Thermodynamics and Molecular Simulation.

(42) Zhao, H.; Xia, S.; Ma, P. Use of ionic liquids as 'green' solvents for extractions. *Journal of Chemical Technology & Biotechnology* **2005**, *80*, 1089–1096.

(43) Jork, C.; Seiler, M.; Beste, Y.-A.; Arlt, W. Influence of Ionic Liquids on the Phase Behavior of Aqueous Azeotropic Systems. *Journal of Chemical & Engineering Data* **2004**, *49*, 852–857.

(44) Zhu, Z.; Ri, Y.; Li, M.; Jia, H.; Wang, Y.; Wang, Y. Extractive distillation for ethanol

dehydration using imidazolium-based ionic liquids as solvents. *Chemical Engineering and Processing - Process Intensification* **2016**, *109*, 190–198.

(45) Ionic liquids as entrainers for water+ethanol, water+2-propanol, and water+THF systems: A quantum chemical approach. *The Journal of Chemical Thermodynamics* **2010**, *42*, 909–919.

(46) Lei, Z.; Dai, C.; Chen, B. Gas Solubility in Ionic Liquids. *Chemical Reviews* **2014**, *114*, 1289–1326.

(47) Zarca Lago, G.; Ortiz Uribe, I.; Urtiaga Mendia, A. M. Novel solvents based on thiocyanate ionic liquids doped with copper(I) with enhanced equilibrium selectivity for carbon monoxide separation from light gases. *Separation and Purification Technology* **2018**, *196*, 47–56.

(48) Zhao, Y.; Gani, R.; Afzal, R. M.; Zhang, X.; Zhang, S. Ionic liquids for absorption and separation of gases: An extensive database and a systematic screening method. *AIChE Journal* **2017**, *63*, 1353–1367.

(49) Seiler, M.; Jork, C.; Kavarnou, A.; Arlt, W.; Hirsch, R. Separation of azeotropic mixtures using hyperbranched polymers or ionic liquids. *AIChE Journal* **2004**, *50*, 2439–2454.

(50) Asensio-Delgado, S.; Pardo, F.; Zarca, G.; Urtiaga, A. Absorption separation of fluorinated refrigerant gases with ionic liquids: Equilibrium, mass transport, and process design. *Separation and Purification Technology* **2021**, *276*, 119363.

(51) Asensio-Delgado, S.; Jovell, D.; Zarca, G.; Urtiaga, A.; Llovell, F. Thermodynamic and process modeling of the recovery of R410A compounds with ionic liquids. *International Journal of Refrigeration* **2020**, *118*, 365–375.

(52) Asensio-Delgado, S.; Viar, M.; Pardo, F.; Zarca, G.; Urtiaga, A. Gas solubility and diffusivity of hydrofluorocarbons and hydrofluoroolefins in cyanide-based ionic liquids for the separation of refrigerant mixtures. *Fluid Phase Equilibria* **2021**, *549*, 113210.

(53) Peng, D.; Zhang, J.; Cheng, H.; Chen, L.; Qi, Z. Computer-aided ionic liquid design for separation processes based on group contribution method and COSMO-SAC model. *Chemical Engineering Science* **2017**, *159*, 58–68, iCAMD – Integrating Computer-Aided Molecular Design into Product and Process Design.

(54) Roughton, B. C.; Christian, B.; White, J.; Camarda, K. V.; Gani, R. Simultaneous design of ionic liquid entrainers and energy efficient azeotropic separation processes. *Computers & Chemical Engineering* **2012**, *42*, 248–262, European Symposium of Computer Aided Process Engineering - 21.

(55) Dowling, A. W.; Vetukuri, S. R. R.; Biegler, L. T. Large-scale optimization strategies for pressure swing adsorption cycle synthesis. *AIChE Journal* **2012**, *58*, 3777–3791.

(56) Dowling, A. W.; Biegler, L. T. A framework for efficient large scale equation-oriented flowsheet optimization. *Computers & Chemical Engineering* **2015**, *72*, 3–20.

(57) Dowling, A. W.; Balwani, C.; Gao, Q.; Biegler, L. T. Optimization of sub-ambient separation systems with embedded cubic equation of state thermodynamic models and complementarity constraints. *Computers & Chemical Engineering* **2015**, *81*, 323–343.

(58) Yokozeki, A.; Shiflett, M. B. Gas solubilities in ionic liquids using a generic van der Waals equation of state. *Journal of Supercritical Fluids* **2010**, *55*, 846–851.

(59) Morais, A. R. C.; Harders, A. N.; Baca, K. R.; Olsen, G. M.; Befort, B. J.; Dowling, A. W.; Maginn, E. J.; Shiflett, M. B. Phase Equilibria, Diffusivities, and Equation of State Modeling of HFC-32 and HFC-125 in Imidazolium-Based Ionic Liquids for the Separation of R-410A. *Industrial & Engineering Chemistry Research* **2020**, *59*, 18222–18235.

(60) Baca, K. R.; Olsen, G. M.; Matamoros Valenciano, L.; Bennett, M. G.; Haggard, D. M.; Befort, B. J.; Garciadiego, A.; Dowling, A. W.; Maginn, E. J.; Shiflett, M. B. Phase Equilibria and Diffusivities of HFC-32 and HFC-125 in Ionic Liquids for the Separation of R-410A. *ACS Sustainable Chemistry & Engineering* **2022**, *10*, 816–830.

(61) Asensio-Delgado, S.; Jovell, D.; Zarca, G.; Urtiaga, A.; Llovell, F. Thermodynamic and process modeling of the recovery of R410A compounds with ionic liquids. *International Journal of Refrigeration* **2020**, *118*, 365–375.

(62) Gmehling, J. Vapor-Liquid Equilibrium Data Collection. *Main, Germany: DECHEMA* **1977**, *chemistry data series: vol. i. Frankfurt*.

(63) Gau, C.-Y.; Brennecke, J. F.; Stadtherr, M. A. Reliable nonlinear parameter estimation in VLE modeling. *Fluid Phase Equilibria* **2000**, *168*, 1–18.

(64) Labarta, J.; Olaya, M. D. M.; Velasco, R.; Serrano, M.; Gomis, A. Correlation of the liquid–liquid equilibrium data for specific ternary systems with one or two partially miscible binary subsystems. *Fluid Phase Equilibria* **2009**, *278*, 9–14.

(65) Costa, A. L. H.; da Silva, F. P. T.; Pessoa, F. L. P. Parameter Estimation Of Thermodynamic Models For High-Pressure Systems Employing A Stochastic Method Of Global Optimization. *Brazilian Journal of Chemical Engineering* **2000**,

(66) Esposito, W. R.; Floudas, C. A. Parameter estimation in nonlinear algebraic models via global optimization. *Computers & Chemical Engineering* **1998**, *22*, S213–S220, European Symposium on Computer Aided Process Engineering-8.

(67) Amaran, S.; Sahinidis, N. V. Global optimization of nonlinear least-squares problems by branch-and-bound and optimality constraints. *Top* **2012**, *20*, 154–172.

(68) Bollas, G. M.; Barton, P. I.; Mitsos, A. Bilevel optimization formulation for parameter

estimation in vapor–liquid(–liquid) phase equilibrium problems. *Chemical Engineering Science* **2009**, *64*, 1768–1783.

(69) Mitsos, A.; Bollas, G. M.; Barton, P. I. Bilevel optimization formulation for parameter estimation in liquid–liquid phase equilibrium problems. *Chemical Engineering Science* **2009**, *64*, 548–559.

(70) Yu, C. Y.; Arnold, D. W. Improved algorithm for obtaining liquid-liquid equilibrium parameters by use of a penalty term. *Industrial & Engineering Chemistry Process Design and Development* **1985**, *24*, 494–498.

(71) Mitsos, A.; Barton, P. I. A dual extremum principle in thermodynamics. *AIChE Journal* **2007**, *53*, 2131–2147.

(72) Hajipour, S.; Satyro, M. A. Uncertainty analysis applied to thermodynamic models and process design – 1. Pure components. *Fluid Phase Equilibria* **2011**, *307*, 78–94.

(73) Hajipour, S.; Satyro, M.; Foley, M. Uncertainty analysis applied to thermodynamic models and process design — 2. Binary mixtures. *Fluid Phase Equilibria* **2014**, *364*, 15–30.

(74) Lee, A.; Ghouse, J. H.; Eslick, J. C.; Laird, C. D.; Siirola, J. D.; Zamarripa, M. A.; Gunter, D.; Shinn, J. H.; Dowling, A. W.; Bhattacharyya, D.; Biegler, L. T.; Burgard, A. P.; Miller, D. C. The IDAES process modeling framework and model library—Flexibility for process simulation and optimization. *Journal of Advanced Manufacturing and Processing* **2021**, *3*, e10095.

(75) Bynum, M. L.; Hackebeil, G. A.; Hart, W. E.; Laird, C. D.; Nicholson, B. L.; Siirola, J. D.; Watson, J.-P.; Woodruff, D. L. *Pyomo–optimization modeling in python*, 3rd ed.; Springer Science & Business Media, 2021; Vol. 67.

(76) Hart, W. E.; Watson, J.-P.; Woodruff, D. L. Pyomo: modeling and solving mathematical programs in Python. *Mathematical Programming Computation* **2011**, *3*, 219–260.

(77) Han, X.; Chen, G.; Cui, X.; Wang, Q. Vapor-Liquid Equilibrium Data for the Binary Mixture Difluoroethane (HFC-32) + Pentafluoroethane (HFC-125) of an Alternative Refrigerant. *Journal of Chemical & Engineering Data* **2007**, *52*, 2112–2116.

(78) Shiflett, M. B.; Yokozeki, A. Vapor-Liquid-Liquid Equilibria of Pentafluoroethane and Ionic Liquid [bmim][PF6] Mixtures Studied with the Volumetric Method. *The Journal of Physical Chemistry B* **2006**, *110*, 14436–14443.

(79) Albà, C. G.; Vega, L. F.; Llovell, F. Assessment on Separating Hydrofluoroolefins from Hydrofluorocarbons at the Azeotropic Mixture R513A by Using Fluorinated Ionic Liquids: A Soft-SAFT Study. *Industrial & Engineering Chemistry Research* **2020**, *59*, 13315–13324.

(80) Reid, R. C. *The properties of gases and liquids*, 4th ed.; McGraw-Hill: New York, 1987.

(81) Klise, K. A.; Nicholson, B. L.; Staid, A.; Woodruff, D. L. In *Proceedings of the 9th International Conference on Foundations of Computer-Aided Process Design*; Muñoz, S. G., Laird, C. D., Realff, M. J., Eds.; Computer Aided Chemical Engineering; Elsevier, 2019; Vol. 47; pp 41–46.

(82) Wächter, A.; Biegler, L. T. On the Implementation of a Primal-Dual Interior Point Filter Line Search Algorithm for Large-Scale Nonlinear Programming. *Mathematical Programming* **2007**, *106*, 25–57.

(83) HSL, A collection of Fortran codes for large scale scientific computation. `http://www.hsl.rl.ac.uk/`, Date of Access: 6/1/2021.

(84) J.P. O'Connell, J. H., J. Paul *Special Distillation Processes*; Thermodynamics: Fun-

damentals and Applications: Cambridge University Press, New York, USA, 2004; pp 421–424.

(85) Burgard, A. P.; Eason, J. P.; Eslick, J. C.; Ghouse, J. H.; Lee, A.; Biegler, L. T.; Millerr, D. C. A smooth, square flash formulation for equation-oriented flowsheet optimization. *Proceedings of the 13th International Symposium on Process Systems Engineering - PSE 2018* **2018**,

(86) Millett G. Morgan, M. H. *Uncertainty: A Guide to Dealing with Uncertainty in Quantitative Risk and Policy Analysis*; Cambridge University: Cambridge, U.K., 1990.

(87) Vasquez, V. R.; Whiting, W. B. Effect of Data Type on Thermodynamic Model Parameter Estimation: A Monte Carlo Approach. *Industrial & Engineering Chemistry Research* **1998**, *37*, 1122–1129.

(88) Wang, J.; Dowling, A. W. Pyomo.DoE: An Open-Source Package for Model-Based Design of Experiments in Python. *AIChE Journal* **2022**, *68*, e17813.

(89) Alkhatib, I. I. I.; Albà, C. G.; Darwish, A. S.; Llovell, F.; Vega, L. F. Searching for Sustainable Refrigerants by Bridging Molecular Modeling with Machine Learning. *Industrial & Engineering Chemistry Research* **2022**, *61*, 7414–7429.